J. Fluid Mech. (1994), vol. 263, pp. 245–270

Flows generated by the periodic horizontal oscillations of a sphere in a linearly stratified fluid

By QIANG LIN, D. L. BOYER AND H. J. S. FERNANDO
Environmental Fluid Dynamics Program, Department of Mechanical and Aerospace Engineering, Arizona State University, Tempe, AZ 85287-6106, USA

(Revised 16 October 1992 and in revised form 27 August 1993)

The flow field induced by a sphere oscillating horizontally in a linearly stratified fluid is studied using a series of laboratory experiments. The resulting flows are shown to depend on the Stokes number β, the Keulegan–Carpenter number KC and the internal Froude number Fr. For $Fr \lesssim 0.2$, it is shown that the nature of the resulting flow field is approximately independent of Fr and, based on this observation, a flow regime diagram is developed in the (β, KC)-plane. The flow regimes include: (i) fully-attached flow; (ii) attached vortices; (iii) local vortex shedding; and (iv) standing eddy pair. An internal-wave flow regime is also identified but, for such flows, the motion field is a function of Fr as well. Some quantitative measures are given to allow for future comparisons of the present results with analytical and/or numerical models. Wherever possible, the results are compared with the experiments of Tatsuno & Bearman (1990) on right circular cylinders oscillating in homogeneous fluids.

1. Introduction

The study of stratified fluid motions past three-dimensional obstacles has potential applications ranging from the motion of ships and submarines in the ocean to the nature of ocean currents past offshore structures or sea-floor topographic features. To better understand the flow past obstacles of complex shapes, it has been traditional to first investigate the flow in similar ranges of parameter space past obstacles of simple shape; e.g. right circular cylinders and spheres. In this spirit the present authors recently investigated steady, linearly stratified flow past a sphere; Lin *et al.* (1992 hereinafter referred to as LLBF). In these experiments the flow relative to the sphere was generated by towing the obstacle horizontally through a fluid at rest with respect to a laboratory observer. The investigation demonstrated the appearance of a rich variety of characteristic flow phenomena as the Reynolds, Re, and Froude, Fi, numbers were varied over a wide range of parameter space; i.e. $5 \lesssim Re \lesssim 10000$ and $0.005 \lesssim Fi \lesssim 20$. Here $Re = U_0 D/\nu$ and $Fi = U_0/DN$, where U_0 is the steady free-stream velocity, D the sphere diameter, N the buoyancy frequency and ν the kinematic viscosity.

One particularly interesting property of the above configuration is that, when the stratification is strong (i.e. $Fi \lesssim 0.2$), and for a range of Re, the flow is approximately horizontal; i.e. in a region of thickness approximately that of the sphere diameter, the flow tends to go around the sphere rather than over it and is, to a reasonable approximation, independent of the vertical coordinate except for thin layers near the top and bottom of the sphere. For example, for $Fe \lesssim 0.2$ and for $100 \lesssim Re \lesssim 500$, vortices with a vertical lengthscale of approximately the sphere diameter are alternately shed in a pattern much the same as that for homogeneous flow past a long vertical circular cylinder having similar Reynolds numbers. For the range $80 \lesssim Re \lesssim 1500$, and

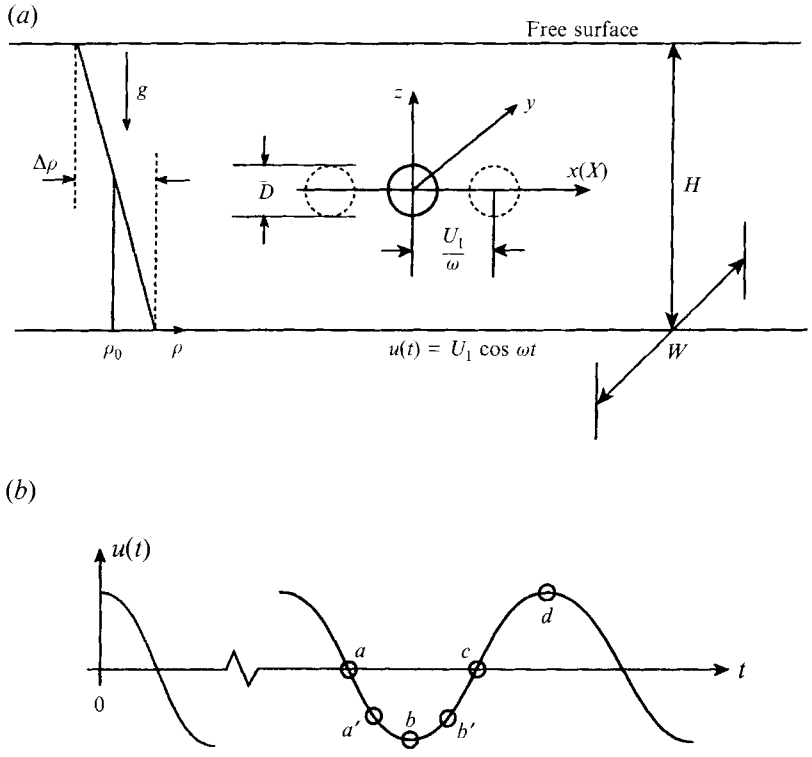

FIGURE 1. (*a*) A physical system. (*b*) Definition of phases *a*–*d* in the sphere oscillation cycle.

for $0.2 \lesssim Fi \lesssim 0.4$, with the lower bound on Fi decreasing somewhat with increasing Re, strong lee waves with overturning motions are observed in the wake of the sphere. In this regime, vortex shedding, as described above, is suppressed. For Froude numbers $Fi \gtrsim 0.4$, a wide variety of interesting flow phenomena are observed whose character depends on both Re and Fi. These higher Re, Fi flows, however, are beyond the scope of the present communication.

The present study deals with the time-dependent motion of obstacles through stratified fluids. In particular, the problem of the horizontal oscillation of a sphere in a linearly stratified fluid is considered in the laboratory. To the authors' knowledge this configuration has not been investigated previously. Numerous studies, however, have been conducted for the case of oscillatory motion of a long cylinder in a homogeneous fluid with the motion direction being perpendicular to the cylinder axis; these include those of Honji (1981), Williamson (1985), Tatsuno & Bearman (1990) and Sarpkaya & Butterworth (1992). Williamson's (1985) study reported laboratory results for a long vertically-oriented circular cylinder oscillating in a rectangular tank. His experiments were for a fixed Stokes number $\beta = 730$ and a range of Keulegan–Carpenter numbers KC given by $0 \leqslant KC < 35$; the findings included the formation of vortex pairs at lower KC with multiple pairings occurring at higher KC values. Tatsuno & Bearman (1990) studied the same problem for a range of Stokes and KC numbers. Their study emphasized the three-dimensional properties of the vortex structures; eight different flow types were delineated. Sarpkaya & Butterworth (1992) investigated the behaviour of the separation angle for cylinders in oscillatory flow. Wang (1965, 1968) and Riley (1966), considered theoretically the motion field resulting from the pure oscillation of a sphere in a homogeneous fluid. The stability of this flow also has been investigated

by Otto (1992). The case of a horizontal circular cylinder oscillating normal and in-line to a uniform horizontal free stream has been studied by Griffin & Ramberg (1974, 1976), Sarpkaya (1986) and Ongoren & Rockwell (1988*a*, *b*). Griffin & Hall (1991) reviewed the issue of vortex shedding lock-on and flow control in bluff-body wakes. Lane (1955) and Nyborg (1953) developed an acoustic streaming theory for flow past a sphere in a homogeneous fluid. Reviews on the shedding of vortices from oscillating bluff bodies have been given by Bearman & Graham (1980) and Bearman (1984).

In a series of laboratory experiments, Zhang & Boyer (1992) considered the nature of the flow in the vicinity of an isolated obstacle of revolution submerged in a linearly stratified fluid in the presence of background rotation. The driving flow was that of a spatially uniform oscillation to simulate some of the effects of tidal currents interacting with undersea mountains. Davies *et al.* (1993) conducted a laboratory investigation of the periodic translation of a horizontal cylinder through a linearly stratified fluid, i.e. the cylinder motion consisted of a periodic streamwise oscillation superimposed on a constant translation. A wide variety of flow types were observed; for example, phenomena such as 'overshooting', as characterized by the wake fluid being advected into the upstream region during certain phases of the flow oscillation, were described.

The focus of the present study is on the physical system depicted in figure 1(*a*). A linearly stratified fluid of mean density ρ_0 and density difference from bottom to top of $\Delta\rho$ is placed in a long tank of width W; the depth of the fluid is H and the upper surface is free. The acceleration due to gravity is g and the kinematic viscosity of the fluid is ν. A sphere of diameter D is placed with its centre at mid-depth and midway between the lateral walls of the tank. The rectangular Cartesian coordinate axes x, y, z are taken relative to the centre of the sphere as indicated. The sphere is then given a sinusoidal oscillation

$$X = \frac{U_1}{\omega}\sin\omega t, \tag{1.1}$$

where X is the displacement of the sphere centre relative to a fixed origin in the tank, U_1 is the maximum sphere speed and ω is the angular frequency.

Assuming that the tank is sufficiently wide (i.e. $W \gg D$) and the fluid sufficiently deep (i.e. $H \gg D$) such that bounding-wall and free-surface effects are unimportant, it is easily shown that the characteristics of the resulting motion depend on three dynamical parameters, namely,

$$KC = \frac{2\pi U_1}{\omega D}, \quad \text{Keulegan–Carpenter number,}$$

$$\beta = \frac{\omega D^2}{2\pi\nu}, \quad \text{Stokes number,}$$

$$Fr = \frac{U_1}{ND}, \quad \text{internal Froude number,}$$

where $N = (g\,\Delta\rho/\rho_0 H)^{\frac{1}{2}}$ is the Brunt–Väisälä frequency. The Keulegan–Carpenter number is the ratio of the amplitude of oscillations to the sphere diameter and the Stokes number represents the ratio of the sphere diameter to the characteristic thickness of the Stokes boundary layer along the sphere surface. The Froude number represents the ratio of the characteristic inertia force due to the sphere oscillations to the buoyancy force.

It is desired to investigate the flow field as a function of KC, β and Fr. Recognizing

the immensity of the task of studying a three-parameter problem in the laboratory, this study focuses primarily on flows at small Froude numbers, i.e. $Fr \lesssim 0.2$, where, based on the steady flow studies of LLBF (and as found in the present experiments), one might expect approximately horizontal flow in the region $-\frac{1}{2}D \lesssim z \lesssim \frac{1}{2}D$. The $Fr \lesssim 0.2$ restriction, as will be shown later, allows one to consider, to a good approximation, the present problem as a two-parameter one involving KC and β. Flows for $Fr \gtrsim 0.2$ will also be discussed briefly. The plan for the paper is to discuss the laboratory facility and techniques in §2, the experimental results in §3 and some conclusions in §4.

2. Experimental facility and techniques

The experiments were conducted in a tank 12.2 m long, 0.4 m wide and 0.3 m high. A computer-controlled towing carriage is mounted on rails located outside the tank and is used to translate model obstacles and experimental accessories along the tank axis. The carriage can be operated in a wide range of time-dependent modes. The maximum speed attainable is 40 cm s^{-1}. The linear stratification of the tank was obtained using a salt-stratified water solution by the well-known Oster (1965) two-tank method. The density profiles were measured by removing fluid samples at designated vertical locations and measuring the density with a refractometer.

The model spheres were supported by thin stainless steel wires (0.04 cm in diameter) passing through the centre of the sphere and connected to diagonally opposite corners of the carriage. On one side, and in front of the carriage, the wire is connected to a support above the water surface while on the other, and behind the carriage, it is attached to the lower portion of a knife-edged support that translates through the fluid near the side of the tank; the knife edge produces minimal disturbances to the working fluid. The support wires were oriented at 17° from the horizontal centreline of the tank. This method of supporting the models minimized (i) the 'sag' that would have occurred by a wire oriented along the channel axis and (ii) the streamwise boundary-layer effects of the wire (see the Appendix of LLBF).

Flow-visualization techniques, including shadowgraphs, dye tracers and neutrally buoyant particle-tracer methods, were employed to investigate the nature of the resulting flow fields. Shadowgraphs were used to obtain side views of the distortion in the density field. The nature of the flow past a sphere is such that the vertical density gradients in localized regions in the wake are significantly stronger than corresponding horizontal ones. Because the shadowgraph technique is more sensitive to sharp changes in the density gradient, top views were not used extensively for flow visualization. Note that in the present application for a sphere, the integrated cross-stream shadowgraph image is not representative of the situation at any cross-section. Thus, shadowgraphs can only give a qualitative picture of the projection of the outer regions of strong density gradients in the wake in the vertical streamwise centreplane.

Polystyrene beads of nominal diameter 0.05 cm and density 1.040 ± 0.005 g cm^{-3} were used as tracer particles. The natural density variation of the particles and background density distribution employed were such as to give a quite uniform particle distribution in the tank. Particle streak photographs were taken in either horizontal or vertical cross-sections by illuminating the tracer particles by a ~ 0.4 cm wide plane light sheet. The light source and camera were either fixed to the carriage or fixed to the tow tank (laboratory frame). Because the experiments considered are mainly for small Fr, the flows are essentially horizontal over the range $-\frac{1}{2}D \lesssim x \lesssim \frac{1}{2}D$; particle streak photographs are thus quite effective in elucidating the motion fields at various elevations. The direction of the fluid motion can be determined from particle streaks

(*a*) Dimensional		(*b*) Non-dimensional	
D (cm)	3.18, 3.81, 5.08	D/H	0.13–0.20
W (cm)	40.2	D/W	0.08–0.13
H (cm)	24–27	KC	0.50–15.1
N (rad s^{-1})	0.94–1.42	β	10.2–175.0
U_1 (cm s^{-1})	0.10–2.00	Fr	0.016–0.39
ω (rad s^{-1})	0.026–0.76		

TABLE 1. Experimental parameters

Figure	D(cm)	U_1(cm/s)	ω(rad/s)	N(rad/s)
1(*a*)	5.08	0.433	0.426	1.23
1(*b*, *c*)	3.81	0.577	0.76	1.10
4	5.08	0.25	0.033	1.24
5	3.81	0.248	0.065	1.12
6	3.81	0.74	0.216	1.42
8	5.08	0.50	0.122	1.05
9	3.17	0.80	0.168	1.42
11	3.81	0.62	0.108	1.15
12(*a*)	3.81	0.79	0.13	1.42
12(*b*)	5.08	0.61	0.06	0.94
13	3.81	0.62	0.108	1.41
15	3.81	0.62	0.108	1.42
19(*a*)	5.08	0.50	0.066	1.24
19(*b*)	3.17	0.80	0.168	1.42
20(*a*)	3.81	0.80	0.13	1.42
20(*b*)	3.17	0.95	0.187	1.42
22	5.08	1.90	0.304	1.20
23	5.08	1.50	0.122	1.05

TABLE 2. Dimensional experimental parameters for photographs presented

by selectively interrupting the light sheet illuminating the particles during the time exposure used to obtain the photographs.

Fluorescein dye was also used for flow visualization. In this method a limited amount of tracer fluid was introduced on the sphere surface using a thin tube after the motion field had reached a quasi-steady state. The tube was then slowly removed from the fluid to minimize disturbances. The resulting patterns of dyed fluid were visualized by the light-sheet previously described. Three acrylic model spheres of diameter 5.08, 3.81 and 3.17 cm were used in the experiments. Typically one hour was allowed between experiments to ensure that background fluid motions in the tank were minimal. Values of the dimensional and dimensionless parameters considered are given in tables 1(*a*) and 1(*b*), respectively. The dimensional parameters for each of the photographs used as illustrations in this communication are given in table 2.

3. Experimental results

The first objective of the experimental programme was to delineate a series of characteristic flow patterns for as wide a range of dimensionless parameter space as possible. To have made this a practicable endeavour, the present study focused on regions of parameter space for which the flow is essentially horizontal in the region

$-\frac{1}{2}D \lesssim z \lesssim \frac{1}{2}D$; i.e. to a good approximation the vertical velocities everywhere were substantially smaller than the horizontal ones. Note that there are transitional horizontal shear layers tangent to the top and bottom of the sphere, where the vortical flows in the range $-\frac{1}{2}D \lesssim z \lesssim \frac{1}{2}D$ adjust rather abruptly to the approximately stagnant external fluid. One exception is the standing eddy pair regime (§3.4) for which the vertical motions in the region $-\frac{1}{2}D \lesssim z \lesssim \frac{1}{2}D$ penetrate $|z| > \frac{1}{2}D$.

Based on the steady flow experiments of LLBF, it is hypothesized that vertical motions in the vicinity of the sphere are negligible under the conditions $Fr \lesssim 0.2$, i.e. phenomena such as lee waves will not be observed. Based on linear wave theory and the experiments of Mowbray & Rarity (1967) for a horizontally oscillating cylinder in a linearly stratified flow at $\omega/N < 1$, one might expect to see wavelike motions, for the present experiments. Note that $\omega/N = 2\pi(Fr/\mathrm{KC})$ and thus, from tables 1 and 2 and the various figure captions, that most of the experiments were conducted for $\omega/N \lesssim 1.0$. While a long cylinder forces vertical motions, which lead to the wave motions observed by Mowbray & Rarity (1967), the sphere at low Fr allows the flow to pass around the obstacle in approximately horizontal patterns. The sphere does not force substantial vertical velocities at $Fr \lesssim 0.2$ and thus is not a good 'wavemaker' for $\omega/N \lesssim 1$.

Assuming then that Fr is relatively unimportant in determining the nature of the flow, the characteristic flows should depend only on KC and β. A KC–β flow regime diagram is thus developed under the restriction $Fr \lesssim 0.2$. The flow character is defined primarily by observations in the horizontal centreplane $z = 0$. In general, the observations are similar in character over most of the depth of the body, except in a thin transition layer near the top and bottom of the sphere. A discussion of the vertical coherence for steady stratified flow past a sphere in the region $-\frac{1}{2}D \lesssim z \lesssim \frac{1}{2}D$ for $Fi \lesssim 0.2$ is given in LLBF. Viscous diffusion is important in the horizontal shear layers along $z \approx \pm\frac{1}{2}D$, where the horizontal motion in $-\frac{1}{2}D \lesssim z \lesssim \frac{1}{2}D$ is separated from the quiescent fluid in $|z| > \frac{1}{2}D$ (except for the long-time behaviour in the standing eddy pair regime), i.e. momentum tends to diffuse rapidly above and below these layers. Observations also lead to the conclusion that the properties of the large-scale structures for the present experiments are similar over the entire depth of the sphere; some small-scale features within the top and bottom horizontal shear layers, on the other hand, are distorted by the shear.

Because of the unsteady nature of the free stream, the flow must be described for various phases of the sphere oscillation. In this regard, principal attention was given to phases a, b, c and d as defined on figure 1(b). Observations in horizontal planes, other than $z = 0$, and in vertical planes oriented along the streamwise direction were also made to clarify the nature of the flow patterns observed. For example, as Fr becomes somewhat larger than 0.2, lee-wave effects become important; these phenomena are demonstrated by observing the motion field in the ($y = 0$)-plane. In the present studies, five quite distinct flow regimes were identified and are discussed below.

3.1. *Fully attached flow*

For sufficiently small KC and for the range of β investigated ($10 \leqslant \beta \leqslant 175$), the flow remains fully-attached to the sphere for all phases of the oscillatory cycle. Figure 2(a) is a particle streak photograph of the horizontal centreplane $z = 0$ obtained by a camera fixed to the tow tank (i.e. the sphere moves with respect to the camera); the exposure time T_e was the time T for one full oscillation cycle of the sphere, between two successive phase a positions. The approximate location of the sphere traverse here, and in the following, is indicated by a sketch at the bottom of the photograph. The bright

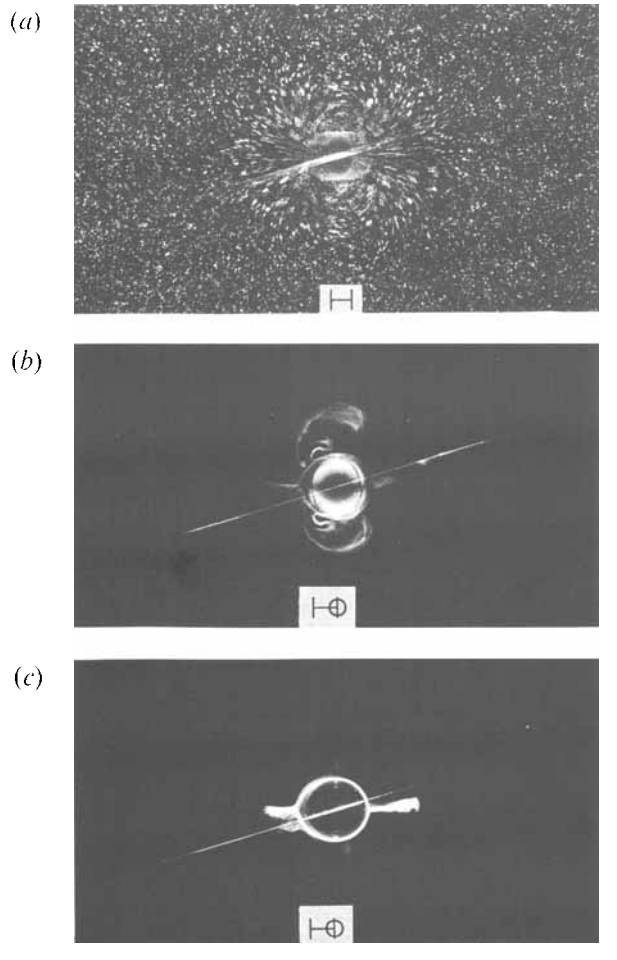

FIGURE 2. Top view of photographs depicting fully attached flow regime for parameter values $\beta = 175$, KC = 1.26 and $Fr = 0.07$; (*a*) particle streaks with camera fixed to tow tank for exposure time $T_e = 1T$ (i.e. from one phase *a* to the next phase *a*), (*b*) dye tracer photograph at phase *a* for observation level $z/D = 0.5$, tracer release time $T_R = 10T$ prior to the photograph; and (*c*) dye tracer photograph at phase *a* for $z/D = 0$, tracer release time $T_R = 15T$ prior to photograph.

oblique line through the centre of the photograph is a reflection from the support wire attaching the sphere to the towing carriage. The dark circular area near the centre of the photograph is the cross-section of the sphere. Because of the small normalized amplitude of oscillation $(U_1/\omega)/D = 0.2$ used in this experiment, the outer edge of the projection of the sphere, while blurred, can be distinguished. Figures 2(*b*) and 2(*c*) are instantaneous horizontal dye tracer photographs taken in planes tangent to the top of the sphere, and through the sphere centre, respectively; the photographs were taken at phase *a* and were approximately 10 and 15 cycles, respectively, after the release of the dye tracer. Figure 2(*b*) shows that the dye tracer in the transitional horizontal shear layer along $z \approx \frac{1}{2}D$ spreads laterally by viscous straining motions.

Figure 2(*c*), taken at phase *a*, indicates that the oscillating sphere for these parameters establishes a weak motion away from the obstacle in the oscillation direction reminiscent of the similar regime for the right circular cylinder found by Tatsuno & Bearman (1990). The photograph of figure 2(*c*) indicates no vortex structures in the lee of the sphere. It is concluded that the flow is 'fully attached' and

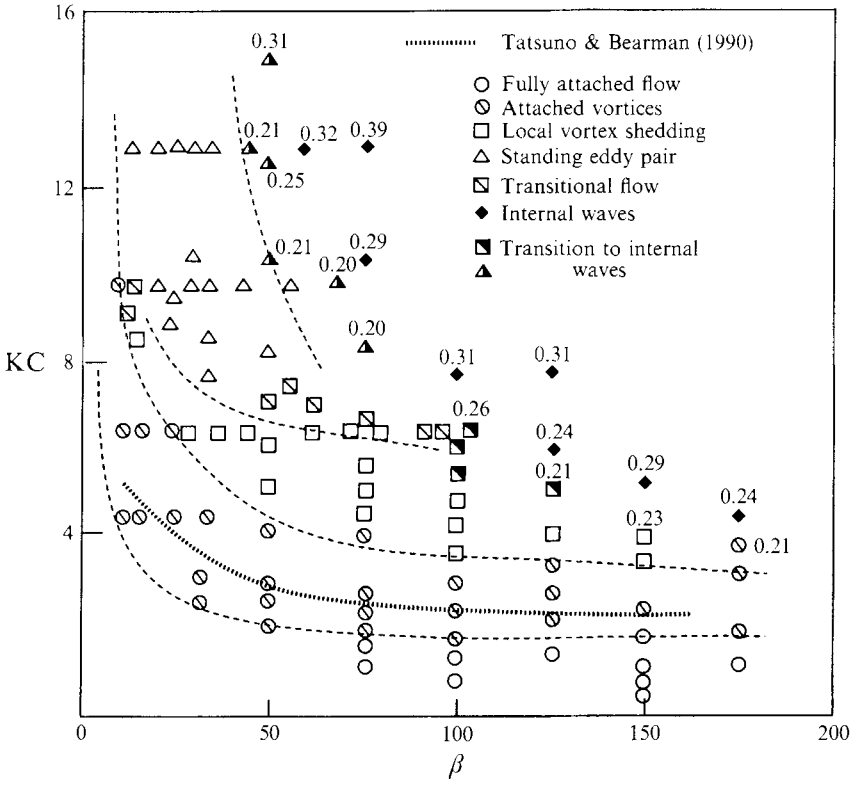

FIGURE 3. Flow regime diagram for KC against β, where numbers above symbols designate values of Fr when $Fr \geqslant 0.20$.

the corresponding flow regime is so designated. The experiments depicted in figure 2 are of relatively low KC (i.e. small normalized oscillation amplitude). The amplitude is not sufficiently large to allow flow separation.

Fully attached flows can also be obtained for large KC and small β. This can be understood by considering experiments with all parameters fixed with the exception of ω. As ω decreases, β decreases. For sufficiently small U_1 then, the flow for small ω (long periods) becomes a slowly varying function of time and the general flow character can be considered as determined by the steady results of LLBF, i.e. fully attached flows can be obtained for sufficiently small ω. Limited numbers of such experiments were conducted in the present programme.

Experiments exhibiting fully-attached behaviour, along with the other flow types to be discussed, are depicted on the regime diagram of figure 3. The dashed lines represent the approximate divisions between the flow regimes, while various symbols indicate the experiments conducted. This diagram is developed based primarily on experiments with $Fr < 0.2$, for which the flow in the region $-\frac{1}{2}D \lesssim z \lesssim \frac{1}{2}D$ is approximately horizontal. Experiments for $Fr > 0.2$, for which strong vertical motions near the sphere are presented, are indicated by a number above the symbol representing the value of Fr. The Froude number effect on the qualitative and quantitative nature of certain flows will be discussed later. It is reiterated that the Froude number Fr varies for the experiments in this diagram; for $Fr \lesssim 0.2$ the flow is approximately horizontal and the effect of variations in Fr on the flow structure is relatively smaller than that from changes in KC and β.

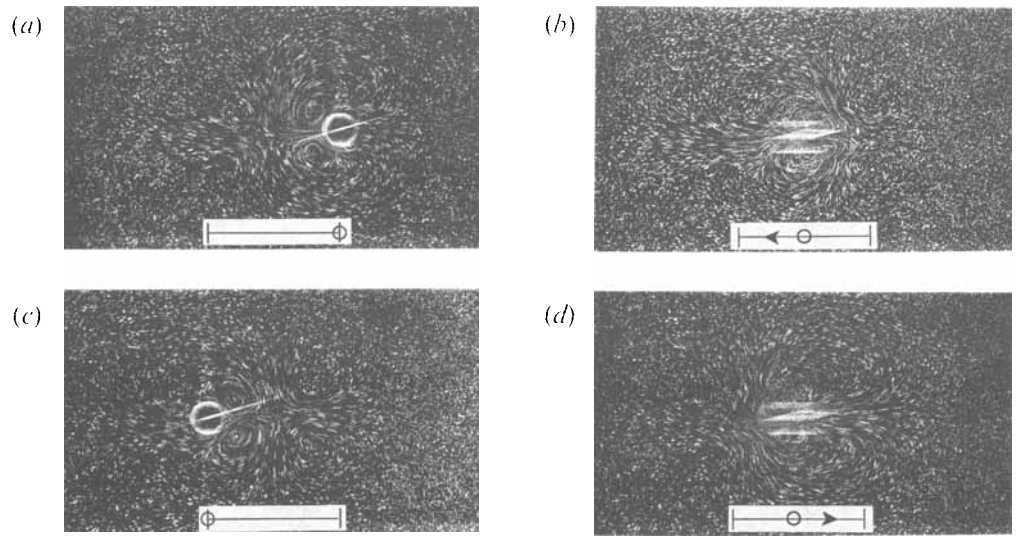

FIGURE 4. Top view of particle streaks in $(z/D = 0)$-plane with camera fixed to tow tank demonstrating attached vortices regime for parameter values $\beta = 13.5$, KC = 9.43, $Fr = 0.04$ and $T_r = 0.10T$; the photographs (*a*)–(*d*) relate to the phase designations as defined in figure 1(*b*).

For a sphere moving (steady or unsteady) in a strongly stratified fluid (i.e. $Fr \lesssim 1$) no blocking is observed, unlike that for a horizontally translating cylinder. In the case of the sphere, the flow can go around the obstacle as shown in LLBF. For a long horizontal cylinder, on the other hand, the flow cannot go around and has insufficient kinetic energy to go over the obstacle and blocking occurs; see, for example, Boyer *et al.* (1989).

It is of interest to compare the current experimental results with other experiments or analytical or numerical models of the same physical system. Unfortunately such studies are unavailable. Owing to the approximately horizontal nature of the flow fields for $Fr \lesssim 0.2$, one can conjecture as to the degree of similarity between strongly stratified flow past a sphere and homogeneous flow past a vertical right circular cylinder. Tatsuno & Bearman (1990, hereinafter referred to as TB) investigated the flow of a homogeneous fluid in the vicinity of an oscillating cylinder for approximately the same ranges of KC and β considered herein; comparisons, where appropriate, are made with these experiments. The approximate boundary in TB between the fully attached regime and the attached vortices regime (§3.2), as estimated from their regime diagram, has a similar shape in the (KC, β)-plane as found herein. Their transition between the two flow regimes, however, occurs at somewhat larger KC (see figure 3). The reason for this discrepancy may be due to the differences in geometry and the criteria used by the two groups in judging flow separation; as pointed out by TB, the boundary between the attached flow and attached vortices regimes cannot be determined clearly.

3.2. *Attached vortices*

As the combination of KC and β is increased beyond the values for fully attached flows, the flow in the vicinity of the sphere, for certain phases of the oscillation cycle, separates from the obstacle. Figures 4(*a–d*) are particle streak photographs, again taken with the camera fixed with respect to the laboratory and in the plane $z = 0$, for this flow regime which is termed 'attached vortices'; the designations *a–d* correspond

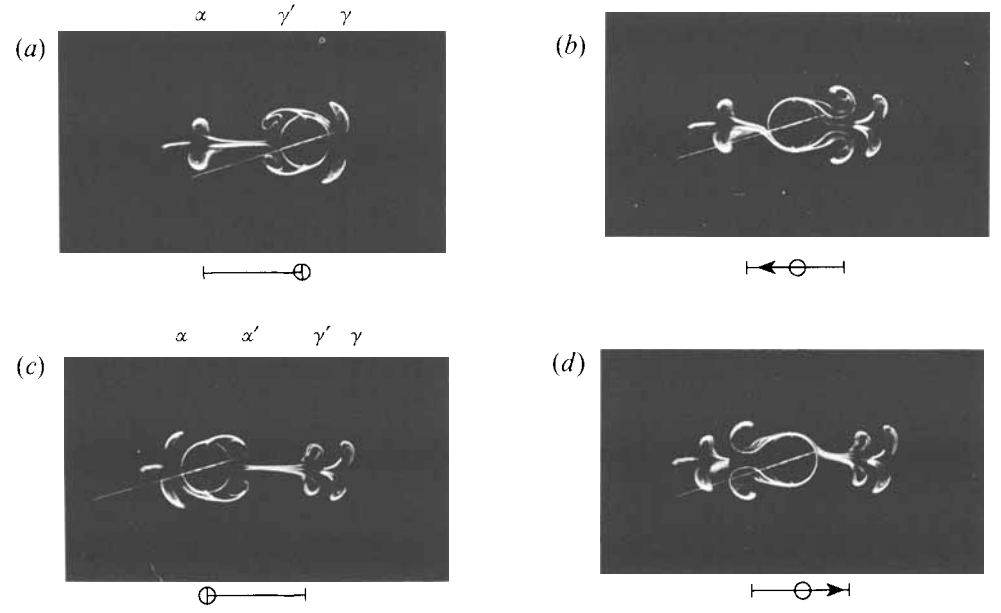

FIGURE 5. Top view of dye tracer photographs in $(z/D = 0)$-plane, demonstrating attached vortices regime for parameter values $\beta = 15$, KC $= 6.28$, $Fr = 0.06$ and $T_R = 1.0T$; see text for definitions of α, α', γ and γ'.

to the phases noted in figure 1(*b*). One notes that at phases *a* and *c*, vortices are clearly visible on the left- and right-hand sides of the sphere, respectively. Phase *a* represents the time for which the free-stream velocity is approximately zero following the left to right trajectory of the sphere thus leading to vortices on the left of the sphere; phase *c* is similar but for the right to left trajectory, with the vortices being on the right. As the sphere translates from right to left from phase *a* to phase *b*, viscous effects, owing to the no-slip condition on the sphere, tend to reduce considerably the strength of the vortices on the immediate left in phase *a*. Thus by phase *c*, the vortices in question are weakened considerably compared to their structure in phase *a*. The same is true for the right-hand side vortices of phase *c* which are seen to be weakened in phase *d*. Similar phenomena for right circular cylinders in homogeneous flows were found by Williamson (1985) and TB.

One question that arises is the fate of the horizontal vorticity component that has the tendency to be produced near the top and bottom (and other portions) of the sphere in the vortex-shedding process; vortices along the top for example will have heavier fluid in their cores while along the bottom the vortex cores will be characterized by lighter fluid, relative to the surroundings. In such circumstances the baroclinic production term in the vorticity equation, $(1/\rho^2)(\nabla\rho \times \nabla p)$, where p is the pressure, can be shown to destroy the horizontal vorticity component both above and below the sphere; see, for example, Van Atta and Hopfinger (1989). Similar arguments also suggest that the horizontal component of the shed vorticity will be destroyed along other portions of the sphere leading to a wake whose vortex structure is principally vertical as is observed in the experiments. Presumably, as the ring vortices shed from the sphere, the vortex line connections between the two truncated vertical vortices diffuse owing to viscous effects.

Figures 5(*a–d*) are dye tracer photographs taken in a horizontal plane through the centre of the sphere at phases *a–d*. In this experiment, a dye tracer has been released

from the surface of the sphere at approximately phase a, one cycle previous to the photograph of figure 5(a), i.e. the photograph is taken at a time $T_R = 1.0\,T$ after release of the dye. As such, the tracer patterns of the left (α) and right (γ) remnant vortex pairs shed during the cycle previous to figure 5(a) are clearly visible and indicated on the top of the photograph; the vortical motion in these structures is weak as observed in particle streak photographs. The sequence given in figure 5 shows clearly the evolution of two new remnant vortex pairs α' and γ', as indicated. By comparing figures 4 and 5, one notes the importance of carefully interpreting dye tracer photographs, since all of the tracer patterns in figure 5 do not depict active vortical structures. Comparing figures 4(c) and 5(c), for example, α is fading, α' is active, γ' has decayed considerably and γ is possibly fossil.

One notes the existence of streamwise motions away from the sphere for all phases of the oscillatory cycle (see figure 4). These are seen to be effectively restricted to within roughly 2–3 diameters of the sphere away from the centre of the sphere trajectory. By comparing these observations with those of TB for a circular cylinder for similar KC and β, respectively, one notes good qualitative agreement with the near field but considerable differences in the far field. That is, the streamwise far field for their experiments indicated a strong streaming motion away from the cylinder, whereas the present results show that the motion field dies quickly away from the sphere in this flow regime. The principal region of flow for the sphere case is restricted to $-\frac{1}{2}D \lesssim z \lesssim \frac{1}{2}D$. This limited vertical extent evidently restricts the streamwise influence distance of the obstacle. Furthermore, the strength of this streaming motion near the sphere in the present experiments is weaker compared with that of a cylinder. For a cylinder, the shear layers occur over the entire length of the cylinder, while for a sphere, this only occurs over a depth of about the sphere diameter.

3.3. *Local vortex shedding*

As the KC, β combination is increased beyond values for the attached vortices regime (see figure 3), vortices were observed to shed from the sphere and the symmetry of the vortex patterns disappeared in a regime termed 'local vortex shedding'. Particle streak photographs demonstrating the nature of this regime are given in figure 6 for a typical period of oscillation; interpretive sketches of these photographs are given in figure 7. Note that this flow may change with time, so that the photographs do not represent a periodic state.

As for the attached vortices regime, at phase a, after the left to right sphere traverse, two counter-rotating eddies α and σ are found in the immediate 'lee'. These vortices have different sizes owing to the influence of the existing motion field; for the case under consideration, σ is larger. Note also in this configuration that there is a left to right asymmetry with the vortex patterns being shifted to the left of the centre of the oscillation trajectory. The relative sizes (strengths) of α and σ depend on the initial instability that leads to the vortices; in other experiments (or for the same experiment at substantially different times), α might be larger than σ. Vortices γ and δ that lie to the left of α and σ, respectively, in phase a, are also apparent with the relative size of γ corresponding to that of α and δ to that of σ. As the sphere translates past α and σ in moving from phase a to phase b, the weaker vortex α is destroyed and 'replaced' by another weak vortex κ of opposite sign, as can be seen at phase c. The destruction of α and formation of κ is due to the generation of clockwise vorticity along the upper portion of the sphere during the right to left traverse. At the same time, vortex σ is weakened by viscous effects (formation of anticlockwise vorticity along the lower portion of the sphere) but because of its original strength maintains its identity,

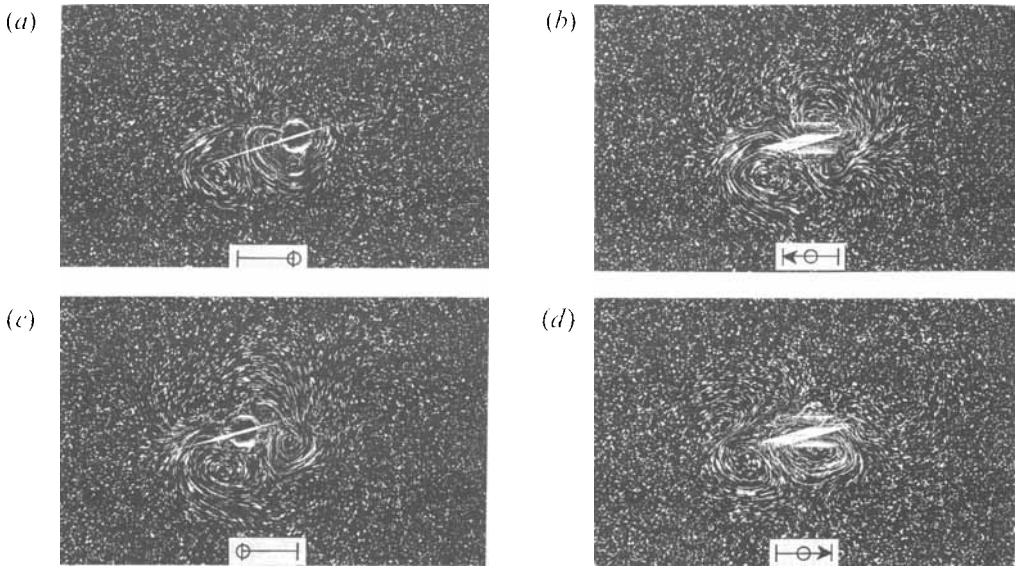

FIGURE 6. Top view of particle streaks in $(z/D = 0)$-plane with camera fixed to tow tank, demonstrating local vortex shedding regime for parameter values $\beta = 50$, KC = 5.65, $Fr = 0.14$ and $T_v = 0.20T$.

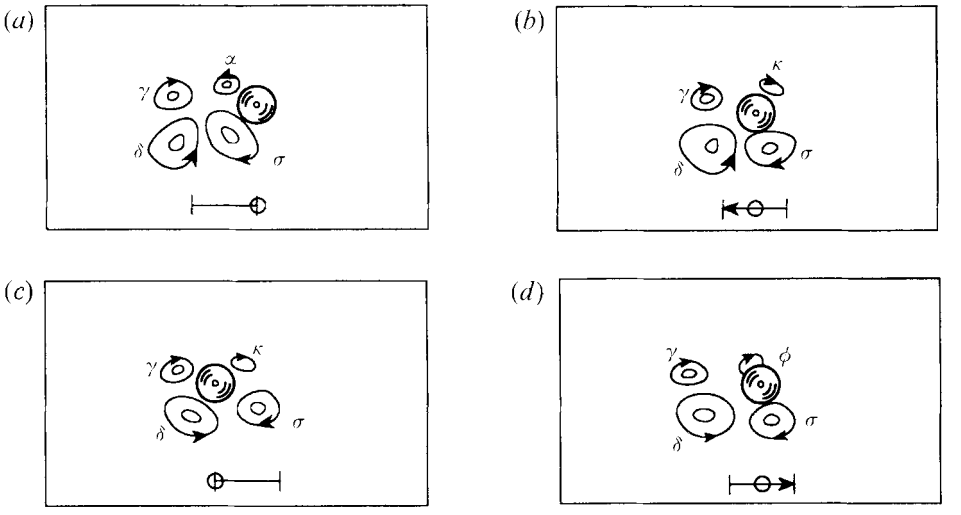

FIGURE 7. Interpretive sketches of photographs of figure 6.

including its sign. By phase c, the weak vortex κ and stronger σ are clearly identifiable. Between phases b and c, γ and δ are strengthened by viscous effects. At phase d, vortex σ is being strengthened and κ being destroyed to be replaced by ϕ (a 'new α') at the next phase a.

It is again emphasized that, depending on the initial instability, the stronger vortices could be found on the upper rather than the lower portions of the flow field. Under this situation the vortex patterns are found to the right of the centre of the sphere oscillation. Furthermore, because of the unstable nature of the flow pattern in the present regime, and experimental irregularities such as residual motions in the tank, the

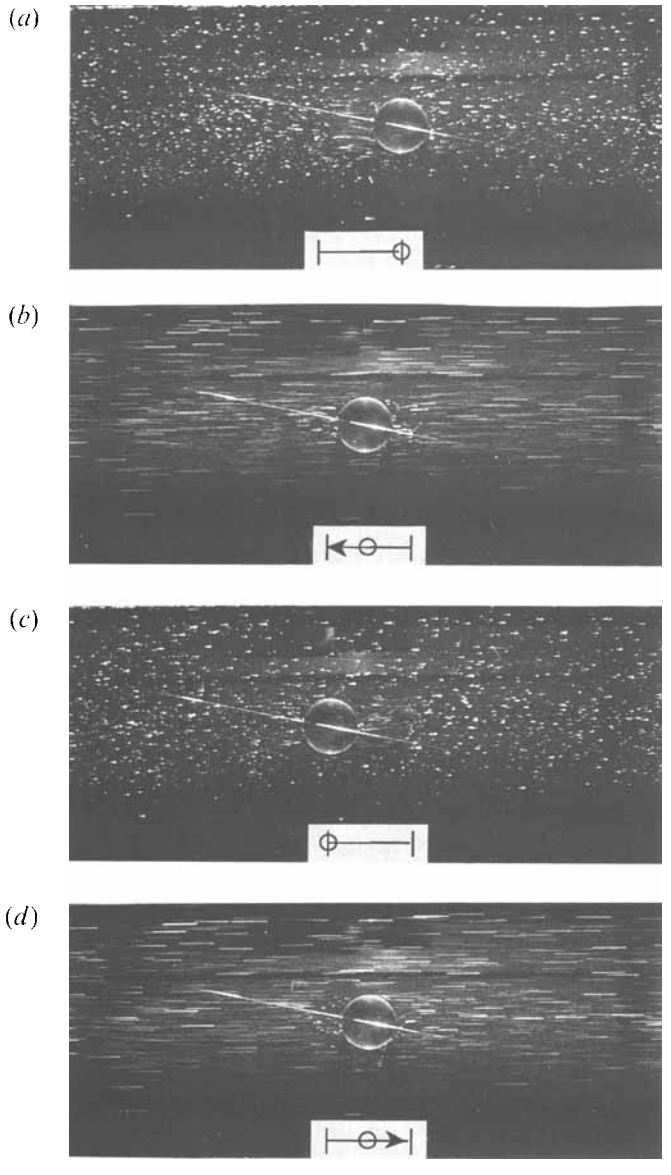

FIGURE 8. Side view of particle streaks in $(y/D = 0)$-plane with camera fixed relative to sphere for local vortex shedding regime for parameter values $\beta = 50$, KC = 5.03, $Fr = 0.09$ and $T_c = 0.11$.

character of the flow, as delineated in figures 6 and 7, can change with time, i.e. the relative strengths α, γ and σ, δ and the 'centre of mass' of the vortex patterns can be reversed from that depicted.

To demonstrate the horizontal nature of the flow, consider figures 8(*a–d*) which are particle streak photographs taken in the $(y = 0)$-plane for an experiment in the local vortex-shedding regime. In contrast to figures 6(*a–d*), which were taken relative to the tank, these photographs are taken relative to an observer fixed to the sphere. The phase *a* and *c* photographs demonstrate the presence of horizontal streamwise motions in the vicinity of the sphere. Owing to the fact that the sphere is at rest at phases *a* and *c*, the tracer particle motions far from the sphere are weak; because the time exposure

includes a short interval during which the sphere is moving, the far-field particle tracers appear as short straight lines. Care must be exercised in interpreting such photographs since the relatively large vortex motions with vertical vorticity near the sphere rapidly advect tracer particles in and out of the vertical light sheet, thus not allowing one to measure the magnitude of the horizontal velocities. The phase b and d photographs also demonstrate the two-dimensional nature of the flow field at this Froude number (i.e. $Fr = 0.09$). The short streaks, or in some cases dots, in the near 'lee' of the sphere are indicative of the presence of substantial lateral motions.

Tatsuno & Bearman (1990) discussed a similar flow pattern for a right circular cylinder; i.e. their regimes D, E. These investigators also found long-term variations in the general flow patterns as found in the present investigation. Again, in contrast to the present experiments, TB found streaming motions away from the cylinder to many diameters in the oscillation direction. Such motions are absent for the sphere as is indicated clearly on figure 6.

3.4. *Standing eddy pair*

For a range of KC $\gtrsim 8$ and for a range of β, as shown on figure 3, one observes a novel characteristic flow termed 'standing eddy pair'. Figures 9 and 10 are particle streak photographs and corresponding interpretive sketches, respectively, depicting the evolution of the motion field in the $(z = 0)$-plane for one oscillation cycle for this regime. The characteristic flow changes with time before reaching a quasi-periodic state in the vicinity of $z = 0$ at roughly 20 oscillation cycles, depending on the system parameters and the region of the flow field being observed. Figures 9 and 10 show the top view of the flow patterns at a time for which the flow in the horizontal centreplane has reached such a quasi-periodic state. Other portions of the flow, however, change slowly with time as discussed below.

The standing eddy pair regime is characterized by two large eddies, i.e. A and B as in figure 10, having vorticity of the same sign and whose centres are located beyond the ends of the sphere traverse. The sign of these eddies depends on the sign of the initial instability, i.e. clockwise for figure 9, but anticlockwise vortices are also possible. As the figures show clearly, the horizontal extent of the standing vortices are substantially larger than the sphere diameter.

Figures 11(a)–11(d) are top views of a time-sequence of dye tracer photographs taken at phases a, a', b and b', where a' is midway between phases a and b and b' is midway between b and c; the light sheet is directed horizontally through the sphere centre. The photograph at phase a was taken 5 oscillations after the tracer release along the surface of the sphere. At each phase and within either the left-hand side or right-hand side standing eddies, the remaining signatures of four to five vortex pairs, as described in the following, can be noted.

Phase a of figures 9, 10 and 11 occurs after the sphere has reached its maximum rightward excursion leaving a relatively strong vortex α in its 'lee' owing to both the shear instability and the background motions; compare the interpretive sketch with the photographs here and in the succeeding discussion. The sphere then moves to the left toward phase b with vortex α advecting past the sphere and interacting with vorticity of the opposite sign in the shear layer of the sphere boundary. Vortex α thus weakens slightly. Furthermore, two counter-rotating vortices δ and σ are initiated 'behind' the sphere as indicated on figure 10(b); these vortices are not clearly observable on figure 9(b) but are on figure 11(b) at phase a'. The horizontal components of the vorticity associated with the shedding of eddies σ and δ are destroyed by baroclinic effects as described previously, i.e. the shed vortex tends initially to be a vertically compressed

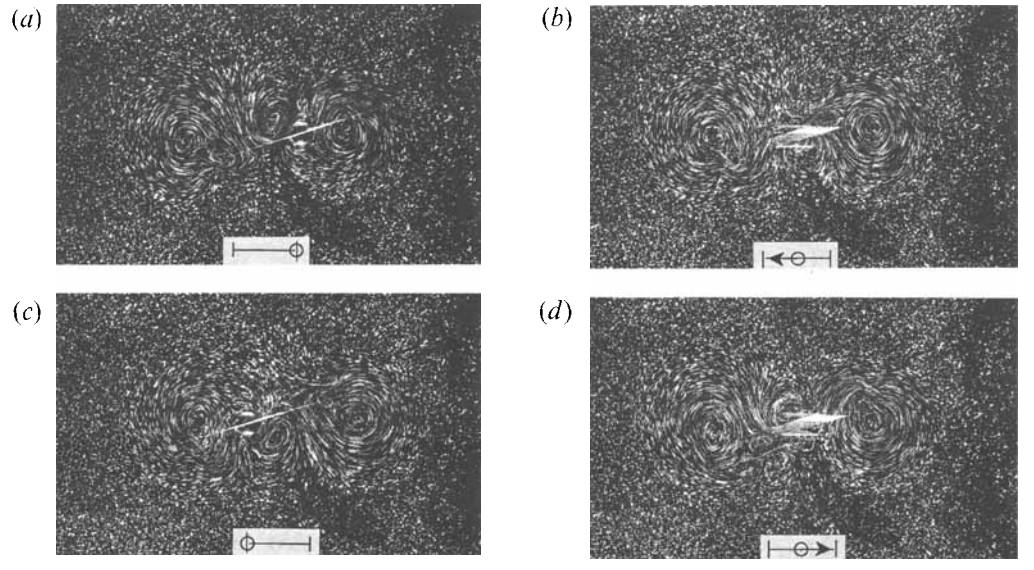

FIGURE 9. Top view of particle streaks in $(z/D = 0)$-plane with camera fixed to tow tank for standing eddy pair regime for parameter values $\beta = 27$, KC = 9.43, $Fr = 0.18$ and $T_e = 0.16T$.

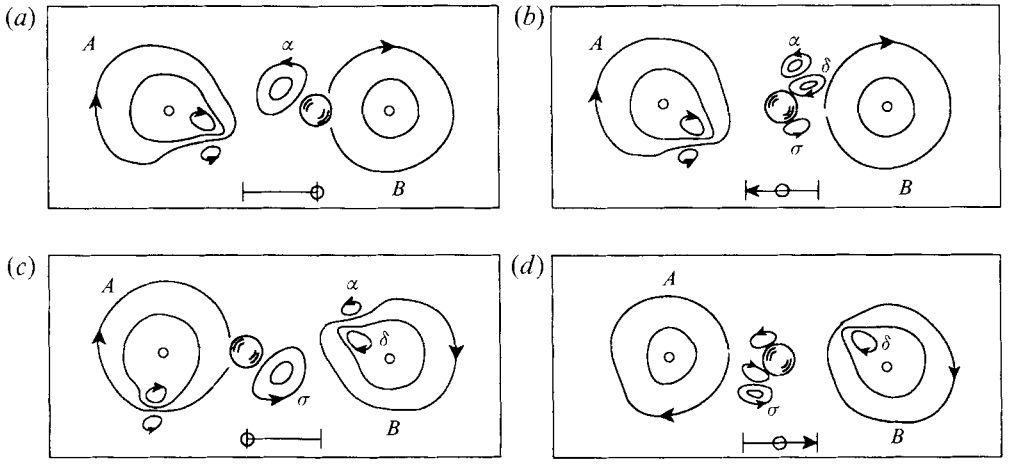

FIGURE 10. Interpretive sketches of photographs of figure 9.

ring owing to stratification (see LLBF) but quickly evolves into two vortices (σ and δ) having essentially only vertical components. Vortices α and δ, being of opposite sign, with δ being somewhat stronger, form a vortex pair and advect downstream. These vortices are then captured by the large right-hand side, standing eddy with vortex α being slowly dissipated from phase c to d and δ being absorbed by the large structure; see the shed vortices being 'incorporated' into the large standing vortices in figure 11. During the motion from phase b to c, anticlockwise vortex σ continues to strengthen. Vortex σ suffers the same fate from phases c to d, as experienced by α in phases a to b, and thus by the next phase a, σ is on the left of the sphere, being absorbed by the left-hand side standing vortex.

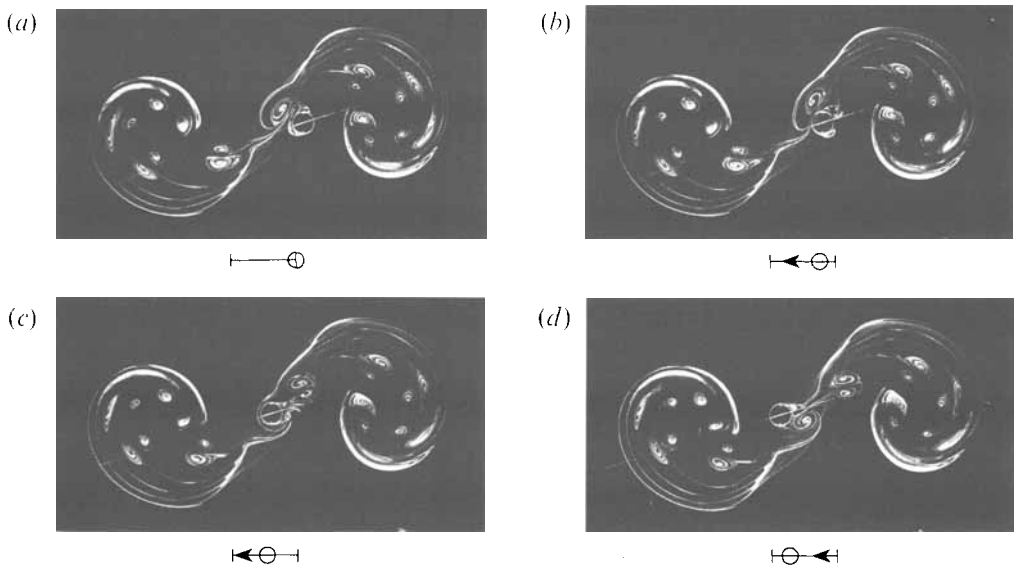

FIGURE 11. Top view of dye tracer photographs in $(z/D = 0)$-plane for standing-eddy pair regime for parameter values $\beta = 25$, KC = 9.43, $Fr = 0.14$ and $T_R = 5$–$6T$. Note that the phases in (*a*)–(*d*) are *a*, *a'*, *b* and *b'*, respectively, as indicated in figure 1(*b*).

Figures 12(*a*) and 12(*b*) are particle tracer photographs taken at phase *a* for two experiments in the standing-eddy pair regime demonstrating that the standing-vortex structures can have different signs depending on the initial conditions of the motion. The standing vortices in figures 12(*a*) and 12(*b*), as indicated, are clockwise and anticlockwise, respectively. Note that the relatively smaller vortices to the immediate left of the sphere in figure 12 have opposite sign to the larger standing vortices. The signs of the vortices in these experiments were observed by eye; alternatively, they could have been determined by chopping the particle streak optically.

One question related to this regime is the time-dependence in the development of the quasi-periodic nature of the flow pattern. In this regard figure 13 is a time sequence of particle streak photographs taken at phase *a*. The first photograph is taken when the sphere first passes through phase *a* (i.e. $t = \frac{1}{4}T$, where T is the period of oscillation). This series of photographs depicts clearly the development and growth of the standing-eddy pairs to a quasi-periodic state in which the standing eddies are continuously fed by the small-scale vortices shed from the sphere during each half oscillation cycle in the manner described above. Since the motion is approximately horizontal, this situation can be construed as an approximate example of two-dimensional vortical turbulence, in which small eddies essentially feed energy to the large eddies which grow with time. However, this flow situation apparently lacks a continuous distribution of small to large scales.

The presence of stratification is crucial to obtaining this characteristic motion. For a sphere oscillating in homogeneous fluids, one might expect ring type vortices to be shed from the sphere. As the amplitude of the sphere velocity became sufficiently large, the vortex ring would become unstable. There would seem to be no mechanism in the homogeneous case to develop standing eddies having relatively large vertical vorticity as shown above for the stratified case. In contrast, one might envisage similar phenomena occurring for oscillating cylinders in homogeneous fluids, i.e. successive shed vortices feeding a standing-eddy pair. Such shed vortices, however, are subject to

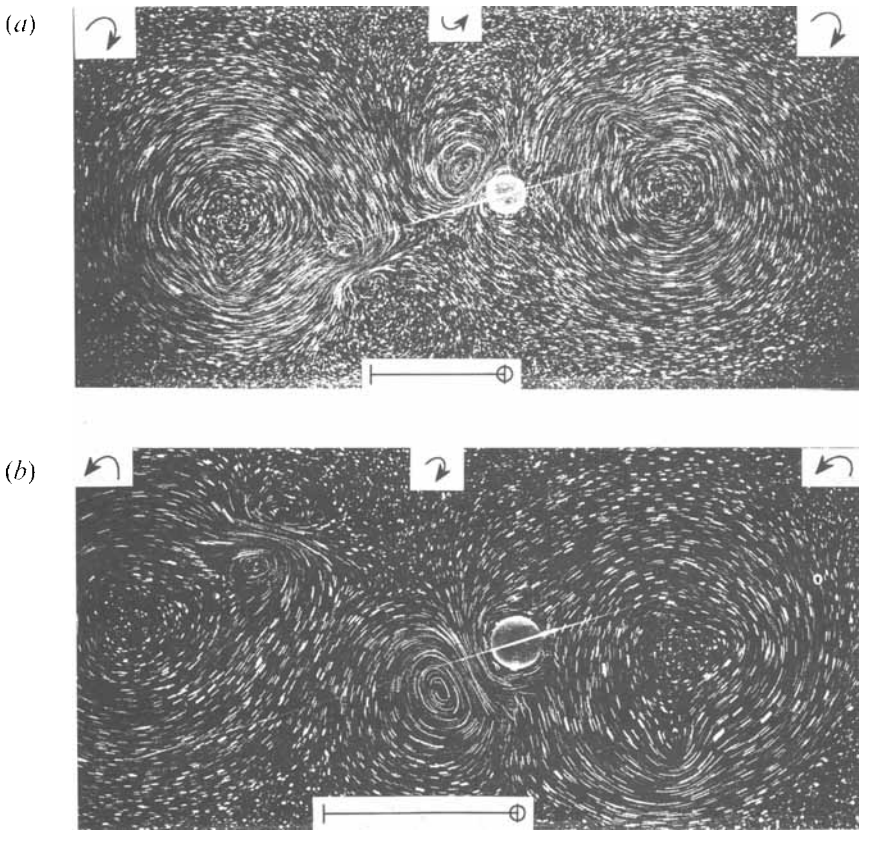

FIGURE 12. Top view of particle streaks in $(z/D = 0)$-plane at phase a for standing-eddy pair regime for (a) clockwise standing eddies, $\beta = 30.0$, KC $= 10$, $Fr = 0.15$ and $T_e = 0.12T$ and (b) anticlockwise standing eddies, $\beta = 24.6$, KC $= 12.6$, $Fr = 0.13$ and $T_e = 0.05T$; the sense of the various vortices is also indicated.

longitudinal instabilities which would tend to preclude observing a standing-eddy pair regime for an oscillating cylinder; see the discussion of TB.

To quantify possible observables for this flow regime, consider the schematic diagram in the lower right corner of figure 14. Define the streamwise distance from the centre of the sphere traverse to the left- and right-hand side standing eddies as X^- and X^+, respectively. Figure 14 is a plot of $|X^-|/D$ and X^+/D against the normalized time since the onset of oscillations, t/T for the experiment depicted in figures 13. The data show a relatively rapid growth in the normalized streamwise location of the eddy structures to an asymptotic value of $X/D \approx 5.0$. Apparently, by about $t/T \approx 20$, the system has reached a quasi-periodic state with respect to the location of the vortices.

To address the question of the vertical structure of the standing eddies, a series of experiments were conducted in which time sequences of particle streak photographs were taken at the observation levels $z/D \approx 3.0$, 2.0, 1.0, 0.5 and 0, respectively. Figures 15(a)–15(d) are selected photographs taken at phase a for four different elevations $z/D \approx 2.0$, 1.0, 0.5 and 0, respectively. Because the vortex strength at $z/D \approx 2.0$ and 1.0 is somewhat weaker than that at $z/D \approx 0.5$ and 0, those photographs (i.e. figure 15a, b) have employed a relatively larger exposure time, so that care must be taken in the quantitative comparisons of figures 15(a)–15(d). It is observed that these large-scale

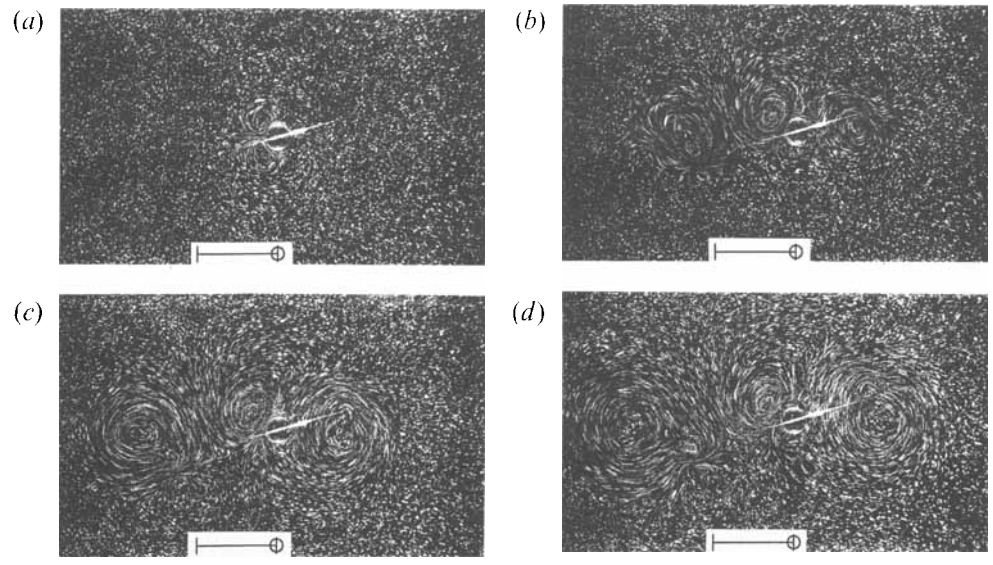

FIGURE 13. Top view of particle streaks in $(z/D = 0)$-plane depicting the temporal development for the standing eddy pair regime at phase a for $\beta = 25$, KC = 9.43, $Fr = 0.11$, $T_e = 0.14T$ and for (*a*) $t \approx 0.25T$, (*b*) $4.25T$, (*c*) $8.25T$, and (*d*) $14.25T$.

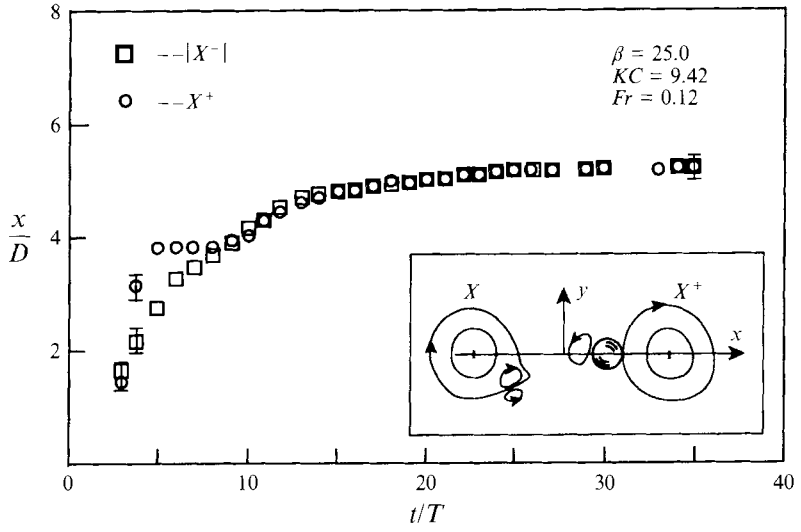

FIGURE 14. Normalized streamwise location of standing eddies against the normalized time t/T for the $(z/D = 0)$-plane.

structures are qualitatively quite the same at different elevations. Because of the temporal nature of the vortex to the immediate left of the sphere in figures 15(*c*) and 15(*d*) (i.e. characteristic time $t/T \sim O(1)$), this short-lived vortex for $|z| \lesssim \frac{1}{2}D$ does not have time to diffuse vertically before it is cancelled by the sphere reversal. This vortex is not observed at elevations $|z| \gtrsim \frac{1}{2}D$ (i.e. figure 15*a*, *b*).

Figure 16 is a plot of the instantaneous normalized velocity distribution V/U_1 obtained from photographs such as figures 15, assuming an axisymmetrical velocity

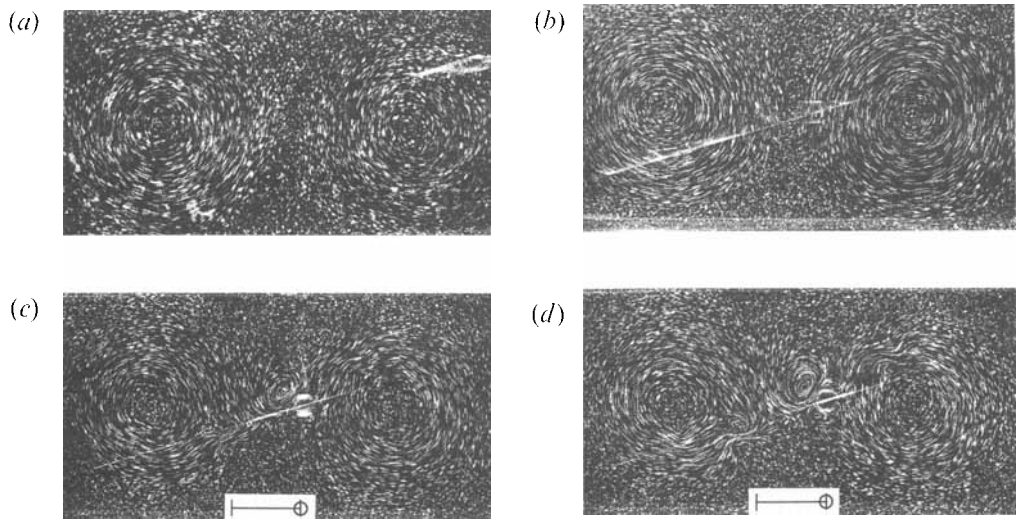

FIGURE 15. Top view of particle streaks for camera fixed to tow tank demonstrating the vortex structure of motion field at different vertical levels for standing eddy pair regime for $\beta = 25$, KC = 9.43, $Fr = 0.11$ and for (*a*) $z/D \approx 2.0$, $T_e = 0.53T$, (*b*) 1.0, $0.34T$, (*c*) 0.5, $0.14T$ and (*d*) 0, $0.14T$.

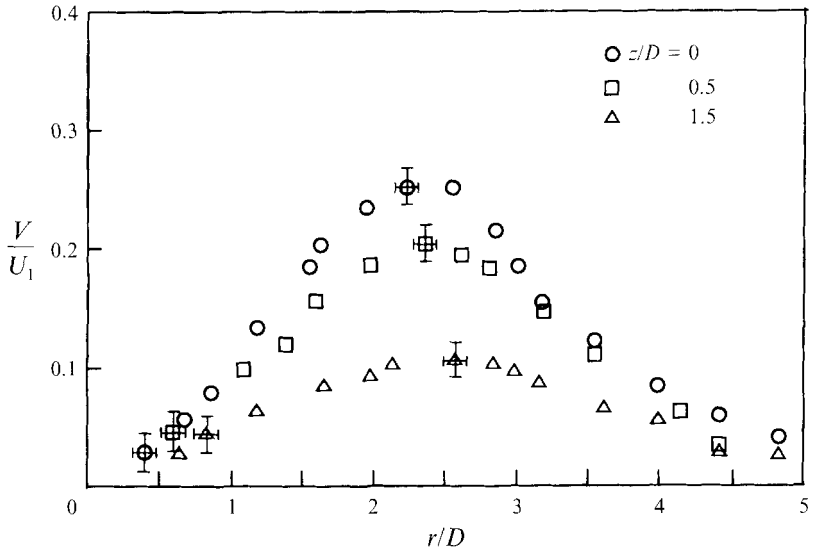

FIGURE 16. Normalized speed of standing eddies against normalized distance from eddy centres for $\beta = 25$, KC = 9.43, $Fr = 0.12$ and the z/D values designated.

distribution; here V is the azimuthal velocity component of the standing eddy. One notes that within the errors of the measurements, the characteristic size of the vortices, as defined by the distance from the centre of the vortex to the location of maximum velocity, is approximately the same at each elevation. The 'eddy size' for this case is estimated to be about $2.2D$. Note again that owing to the quasi-steady nature of this standing-eddy structure, the eddies found in the layer $|z| \lesssim \frac{1}{2}D$ can drive steady vortical motions to large distances vertically. This phenomena, however does not occur for

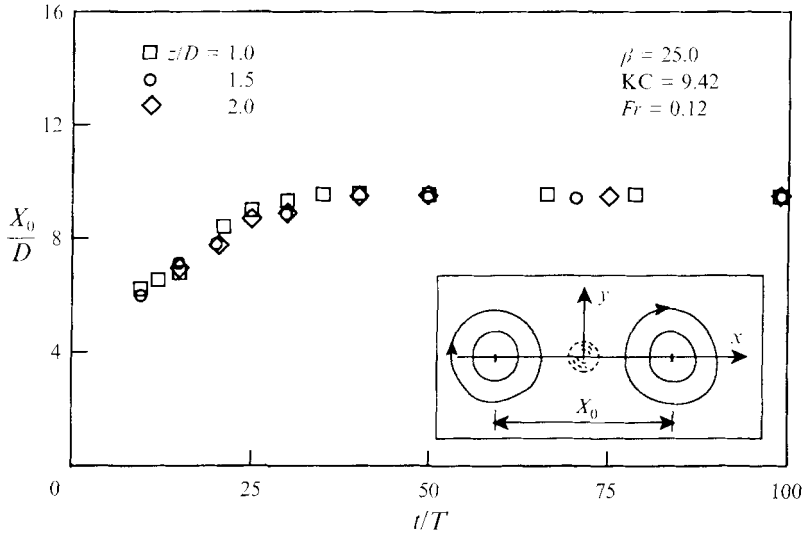

FIGURE 17. Normalized separation distance of standing eddies against the normalized time for $\beta = 25$, KC = 9.42, $Fr = 0.12$ and the z/D designated.

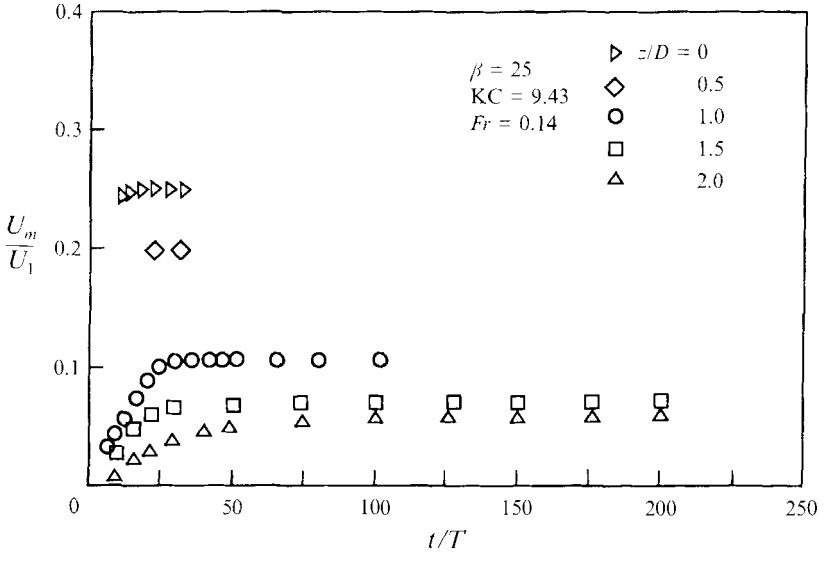

FIGURE 18. Normalized maximum speed of the standing eddies against the normalized time for $\beta = 25$, KC = 9.43, $Fr = 0.14$ and the z/D designated.

other flow regimes for which large-scale eddy structures do not appear as quasi-steady features of the flow field.

Figure 17 is a plot of the normalized standing vortex separation distance X_0/D as defined in the insert, for the sequences of observations for the experiments exemplified by figures 15. As noted again, within the limits of the observations, the vortex separation distance is independent of height. The standing vortices are thus vertically coherent, as relates to both their streamwise location (figure 17) and size (figure 16). Finally, figure 18 is a plot of the normalized maximum speed U_m/U_1 of the standing eddies at various elevations as a function of the normalized time t/T (here U_m is estimated by choosing the longest streakline along the azimuthal direction). As might

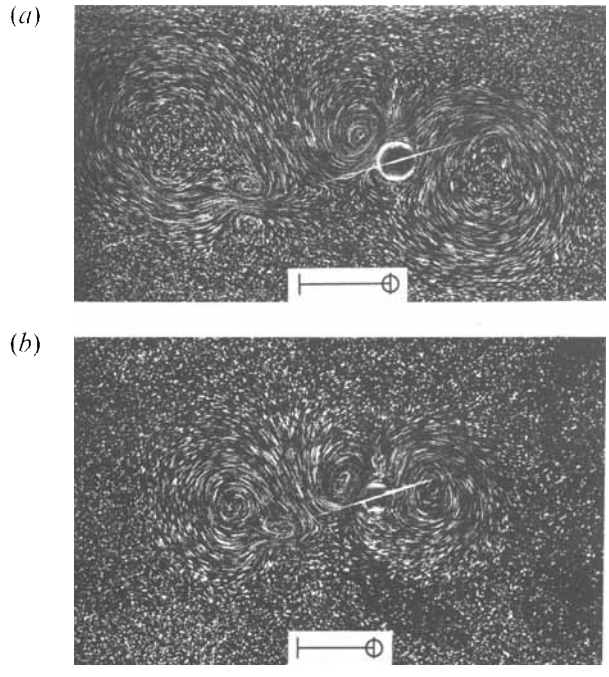

FIGURE 19. Top view of particle streaks in $(z/D = 0)$-plane showing the variation of streak patterns with Froude number for the standing eddy pairs regime at phase a for $\beta = 27$, KC = 9.43 and for (a) $Fr = 0.08$, $T_r = 0.10$ and (b) 0.18, 0.21.

be expected, the eddy strength given by U_m/U_1, decreases with increasing observation level. Furthermore, the eddy structures approach a quasi-steady state, with the time required to reach this point increasing with increasing observation level.

At very large times (e.g. $t/T \sim 200$ for the experiments in figure 15) one observes that the respective standing vortices induce a small motion field on each other. There is thus a tendency for the standing vortices to rotate in a clockwise sense. This motion, however, cannot continue since the character of this flow regime could not be maintained. Furthermore sidewall effects become important as the size of the standing eddies reaches a significant fraction of the tank width.

Tatsuno & Bearman (1990) discussed a flow pattern in a similar β–KC range for an oscillating circular cylinder (their regime F) which had some similarities to the standing-eddy pair flow regime in the present experiments. In particular, the shed vortex pairs travelled in a straight path to large distances away from the cylinder. The dye tracer photographs for their regime F, however, do not indicate the formation of large-scale standing eddies. Furthermore the structure of their shed eddies is subject to three-dimensional breakdown. The standing-eddy pair regime thus appears to depend crucially on the presence of stratification.

For $Fr \lesssim 0.20$, experiments in the standing-eddy pair regime indicate that the flow fields are qualitatively similar for fixed β and KC and varying Fr. Figure 19 exemplifies this observation for experiments at fixed $\beta = 27$, KC = 9.43, and for $Fr = 0.08$ and 0.18; both photographs are taken at phase a. A closer analysis of such photographs, however, shows that there are some small quantitative differences. Figure 20, for example, is a plot of $|X^-|/D$ and X^+/D against Fr for a number of experiments for selected β, KC combinations taken after the flow reached a quasi-steady state. It is observed that for low Fr, while keeping β and KC constant (e.g. the circles), the normalized distances remain approximately constant; at large Fr, the distances

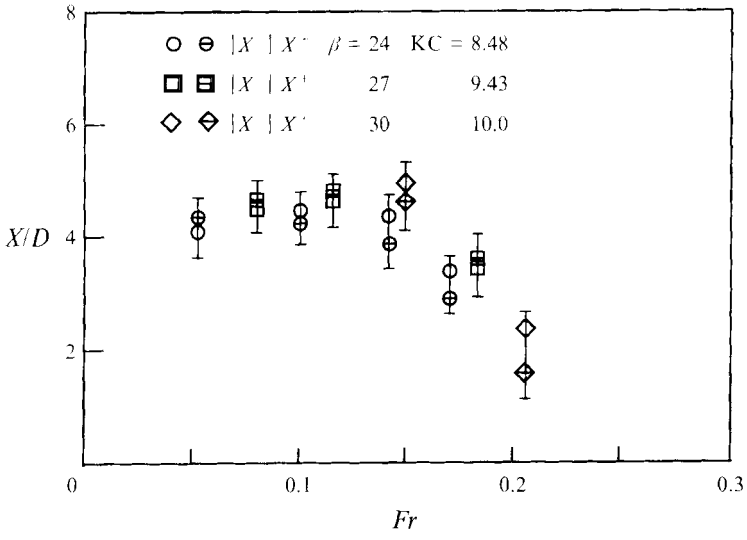

FIGURE 20. Normalized streamwise locations of standing eddies against Froude number in $(z/D = 0)$-plane for the designated parameters.

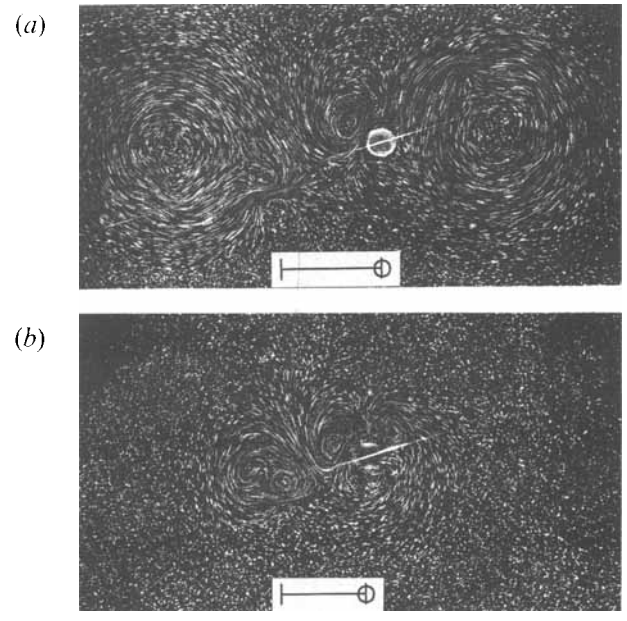

FIGURE 21. Top view of particle streaks in $(z/D = 0)$-plane at phase a demonstrating diminution of standing eddy pair for $Fr \gtrsim 0.20$; parameter values are $\beta = 30$, KC = 10.0 and for (*a*) $Fr = 0.15$, $T_c = 0.12$, and (*b*) 0.21, 0.18.

decrease as vertical motions become dominant. Based on the measurements of figure 20, it is concluded that the Froude number has an effect on the quantitative properties of the flow for $0.15 \lesssim Fr \lesssim 0.20$. As the Froude number is increased above 0.2, substantial vertical motions are observed in the vicinity of the sphere and the flows can no longer be assumed approximately horizontal.

Experiments at fixed β and KC for $Fr \lesssim 0.2$ and $Fr \gtrsim 0.2$, respectively, indicate the dramatic change in flow structure occurring in the vicinity of this critical $Fr \approx 0.2$. For

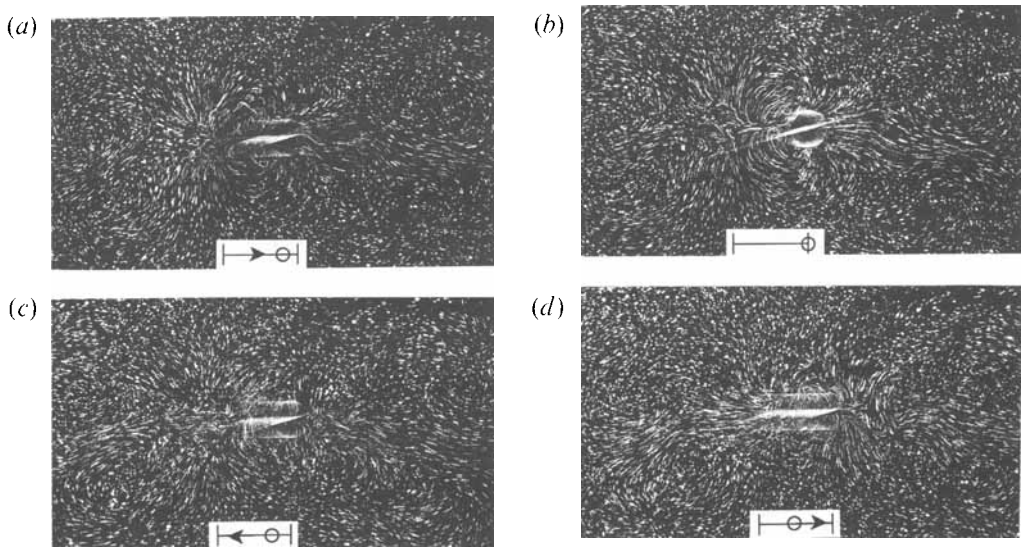

FIGURE 22. Top view of particle streaks in $(z/D = 0)$-plane for camera fixed to tow tank for internal wave regime for parameter values $\beta = 125$, KC = 7.85, $Fr = 0.31$ and $T_e = 0.19$; the approximate phases are indicated with (*b*) corresponding to phase *a*.

example, figures 21 (*a*) and 21 (*b*) depict particle streak photographs for the horizontal centreplane $z = 0$ for experiments at fixed $\beta = 30.0$, KC = 10.0, with different $Fr = 0.15$ and 0.21, respectively. The photographs, taken at phase *a*, show clearly that the standing eddy pair structure is effectively destroyed for the larger Fr case. This is due to the strong vertical motion (internal waves) inherent in $Fr \gtrsim 0.2$ experiments, i.e. the accompanying internal waves are of critical importance in determining the large-scale features of the flow.

Flows for which vertical motions are important are termed the internal wave regime; the regime is characterized by the absence of closed horizontal vortex patterns. Before the flow enters the internal wave regime, there is a fair range of KC, β over which transitional flow is observed (figure 3). In this range, the standing eddies are weak but the vertical motion is not pronounced enough to generate strong internal waves to fully suppress horizontal vortex shedding. Such experiments are indicated on the regime diagram by semi-filled symbols.

3.5. *Internal waves*

As noted above, for Froude numbers $Fr \gtrsim 0.2$, vertical motions become important and the flow can no longer be assumed to be approximately horizontal. The resulting flow regimes thus depend not only on KC and β, but on Fr as well. No attempt was made in the present study to develop a regime diagram in this three-dimensional parameter space. Nevertheless a number of case studies were considered. For very large Fr (i.e. $Fr \gtrsim 0.30$) the flow field is characterized by complex motions with no closed vortex structures; see, for example, the photographs given in figure 22. Here horizontal particle streak photographs have been taken, with the camera fixed to the laboratory frame. Shorter phase intervals have been employed to determine the presence of possible closed horizontal vortex structures. As the photographs show clearly, no well-defined closed vortex structures occur. Note that in figure 22, the particles may move in and out of the horizontal light sheet owing to the non-zero vertical velocity caused

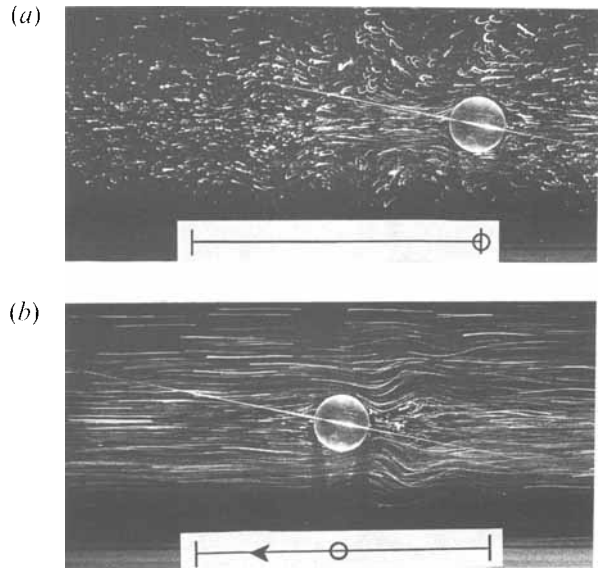

FIGURE 23. Side view of particle streaks in $(y/D = 0)$-plane for camera fixed relative to sphere for internal wave regime for parameter values $\beta = 50$, KC = 15.2, $Fr = 0.28$ and $T_r = 0.08T$.

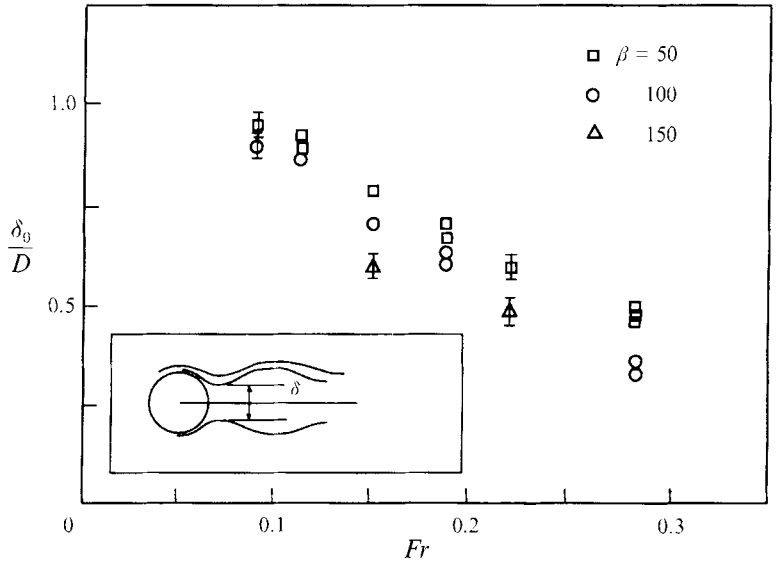

FIGURE 24. Normalized height of pinched region δ_0/D against Fr for internal wave regime and for the β values indicated.

by strong internal waves. In some experiments closed vortex structures have been observed in the $z = 0$ plane for $Fr \lesssim 0.30$.

The flow at large Froude numbers is dominated by internal waves as can be noted on the vertical particle streak photographs along $y = 0$, as shown in figure 23; phases c and d are not shown because they are virtually identical to a and b, respectively, with $x \to -x$. The presence of three-dimensional motions at all depths in the vicinity of the sphere traverse is evident. Phase b corresponds to the maximum velocity of the sphere, and shows clearly, a strong 'lee'-wave pattern throughout the bulk of the fluid. These strong vertical motion effects bring into play the importance of Fr, as well as β and KC, in determining the nature of the flow field.

Figure 24 shows the results of measurements of the normalized pinched height δ_0/D; here δ_0 is defined as the minimum distance between streamlines in the near lee passing over and under the sphere, as shown in the insert. The general trend shows that the normalized height decreases with Fr and by $Fr \approx 0.2$, the pinched region $\delta_0/D \approx 0.7$; i.e. the value of Fr for which vertical velocity effects become important. Also shown is the effect of β on the pinched height, where δ_0/D is smaller for larger values of β at fixed Fr. As β increases, the oscillation frequency ω approaches the buoyancy frequency N, and consequently the phase velocity of the waves become more nearly horizontal; this in turn allows for larger vertical excursions of the fluid parcels.

It must again be emphasized that the regime diagram of figure 3 depends crucially on maintaining $Fr \lesssim 0.2$. For example, should Fr be raised above this level for any of the KC and β experiments for the regimes discussed in §§3.1–3.5, internal wave effects would be important and thus the regimes noted in figure 3 may not be observed.

4. Concluding remarks

Experiments on the motion field formed by the periodic horizontal oscillation of a sphere in a linearly stratified fluid have been conducted. The resulting characteristic flows depend on the Keulegan–Carpenter number KC, the Stokes number β, and the internal Froude number Fr. The most important findings of the study include:

1. For $Fr \lesssim 0.2$, the flow field is approximately horizontal; the nature of the observed flow thus depends primarily on KC and β. A KC against β flow regime diagram, based principally on the observations of the flow field in the horizontal centreplane $z = 0$, was developed. This includes flow types termed: (i) fully-attached flow; (ii) attached vortices; (iii) local vortex shedding; and (iv) standing eddy pair flow regimes.

2. For $Fr \gtrsim 0.2$, vertical motion in the form of internal waves becomes important with the character of the resulting motion field determined by three parameters KC, β and Fr. For $Fr \gtrsim 0.3$, and for the range of KC and β considered, vortical structures with closed streamlines in the $(z = 0)$-plane are not observed at any phase in the sphere oscillation cycle.

3. The motion field for the fully-attached flow, attached vortices and for the local vortex shedding regimes is confined principally to the vertical layer $-\frac{1}{2}D \lesssim z \lesssim \frac{1}{2}D$.

4. The standing-eddy pair regime is found to be unique in the sense that strong, quasi-permanent vortex structures are formed beyond each end of the sphere trajectory. Both vortices have the same sign as determined by the initial instability that leads to their formation. These standing eddies induce vortical motion throughout the fluid column (i.e. in regions beyond $|z/D| > 0.5$) through viscous diffusion. The temporal and spatial development of these structures for certain case studies were presented.

5. For $Fr \lesssim 0.20$ and for the β and KC investigated, the qualitative properties of the flow are similar for a given pair of KC and β. In the range $0.15 \lesssim Fr \lesssim 0.20$, some quantitative measures (for a fixed pair of KC and β) are affected by the buoyancy effects.

6. Despite the difference in geometry, the regime diagram determined for stratified flow past a sphere has some characteristics similar to those for a right circular cylinder oscillating in a homogeneous flow, as investigated by Tatsuno & Bearman (1990).

The authors would like to express their gratitude to the support of the Office of Naval Research under its Accelerated Research Initiative on Vortex Dynamics, Grant No. N00014-90-J-4063 and the National Science Foundation (Fluid Mechanics & Hydraulics Program).

REFERENCES

BEARMAN, P. W. 1984 Vortex shedding from oscillating bluff bodies. *Ann. Rev. Fluid Mech.* **16**, 195–222.

BEARMAN, P. W. & GRAHAM, J. M. R. 1980 Vortex shedding from bluff bodies in oscillatory flow: a report on Euromech 119. *J. Fluid Mech.* **99**, 225–245.

BOYER, D. L., DAVIES, P. A., FERNANDO, H. J. S. & ZHANG, X. 1989 Linearly stratified flow past a horizontal circular cylinder. *Phil. Trans. R. Soc. Lond.* A**328**, 501–528.

DAVIES, M. E. 1976 A comparison of the wake structure of a stationary and oscillating bluff body, using a conditional averaging technique. *J. Fluid Mech.* **75**, 209–231.

DAVIES, P. A., BOYER, D. L., FERNANDO, H. J. S. & ZHANG, X. 1993 On the unsteady motion of a circular cylinder through a linearly-stratified fluid. *Phil. Trans. R. Soc. Lond.* in press.

GERRARD, J. H. 1966 The mechanics of the formation region of vortices behind bluff bodies. *J. Fluid Mech.* **25**, 401–413.

GRIFFIN, O. M. & HALL, M. S. 1991 Review – vortex shedding lock-on and flow control in bluff body wakes. *Trans ASME I: J. Fluids Engng* **113**, 526–537.

GRIFFIN, O. M. & RAMBERG, S. E. 1974 The vortex-street wakes of vibrating cylinders. *J. Fluid Mech.* **66**, 553–576.

GRIFFIN, O. M. & RAMBERG, S. E. 1976 Vortex shedding from a cylinder vibrating in line with an incident uniform flow. *J. Fluid Mech.* **75**, 257–271.

HONJI, H. 1981 Streaked flow around an oscillating circular cylinder. *J. Fluid Mech.* **107**, 509–520.

LANE, C. A. 1955 Acoustic streaming in the vicinity of a sphere. *J. Acoust. Soc. Am.* **27**, 1082.

LIN, Q., LINDBERG, W. R., BOYER, D. L. & FERNANDO, H. J. S. 1992 Stratified flow past a sphere. *J. Fluid Mech.* **240**, 315–355.

MOWBRAY, D. E. & RARITY, B. S. 1967 A theoretical and experimental investigation of the phase configuration of internal waves of small amplitude in a density stratified fluid. *J. Fluid Mech.* **28**, 1–16.

NYBORG, W. L. 1953 Acoustic streaming due to attenuated plane waves. *J. Acoust. Soc. Am.* **25**, 68–75.

ONGOREN, A. & ROCKWELL, D. 1988*a* Flow structure from an oscillating cylinder. Part 1. Mechanisms of phase shift and recovery in the near wake. *J. Fluid Mech.* **191**, 197–223.

ONGOREN, A. & ROCKWELL, D. 1988*b* Flow structure from an oscillating cylinder. Part 2. Mode competition in the near wake. *J. Fluid Mech.* **191**, 225–245.

OSTER, G. 1965 Density gradients. *Sci. Am.* **213**, 70–76.

OTTO, S. R. 1992 On the stability of flow around an oscillating sphere. *J. Fluid Mech.* **239**, 47–63.

RILEY, N. 1966 On the sphere oscillating in a viscous fluid. *Q. J. Mech. Appl. Maths* **19**, 461–472.

SARPKAYA, T. 1986 Force on a circular cylinder in viscous oscillatory flow at low Keulegan–Carpenter numbers. *J. Fluid Mech.* **165**, 61–71.

SARPKAYA, T. & BUTTERWORTH, W. 1992 Separation points on a cylinder in oscillating flow. *Trans. ASME: J. Offshore Mech. Arc. Engng* **114**, 28–35.

TANEDA, S. 1991 Visual observations of the flow around a half-submerged oscillating sphere. *J. Fluid Mech.* **227**, 193–209.

TATSUNO, M. & BEARMAN, P. W. 1990 A visual study of the flow around an oscillating circular cylinder at low Keulegan–Carpenter numbers and low Stokes numbers. *J. Fluid Mech.* **211**, 157–182.

VAN ATTA, C. W. & HOPFINGER, E. J. 1989 Vortex ring instability and collapse in a stably stratified fluid. *Exps Fluids* **7**, 197–200.

WANG, C. 1965 The flow field induced by an oscillating sphere. *J. Sound Vib.* **2**(3), 257–269.

WANG, C. 1968 On high-frequency viscous flows. *J. Fluid Mech.* **32**, 55–68.

WILLIAMSON, C. H. K. 1985 Sinusoidal flow relative to circular cylinders. *J. Fluid Mech.* **155**, 141–174.

ZHANG, X. & BOYER, D. L. 1992 Motion of oscillatory currents past isolated topography. *J. Phys. Oceanogr.* **20**(9), 1425–1448.